https://doi.org/10.5194/sand-2026-3
Preprint. Discussion started: 25 March 2026

SaND
Safety of Nuclear Waste Disposal
Discussions

The role of gas injection rate on the advective movement of gas in Opalinus Clay at the field scale

Robert Cuss[1], Jocelyn Gisiger[2], Antonio Pio Rinaldi[3], Elliot Bird[1], David Jaeggi[4], Matthijs Nuus[3], Manuel Sentis[5], Bastian Graupner[5], Frédéric Bernier[6], Fabien Magri[7], Jon Harrington[1]

[1]British Geological Survey (BGS), Keyworth, Nottingham, NG12 5GG, UK
[2]Solexpers AG, Mönchaltdorf, Switzerland
[3]Swiss Seismological Service, Department of Earth and Planetary Sciences, Swiss Federal Institute of Technology in Zurich (ETH), Zurich, Switzerland
[4]Federal Office of Topography (swisstopo), Route de la Gare 63, 2882, St-Ursanne, Canton of Jura, Switzerland
[5]Swiss Federal Nuclear Safety Inspectorate (ENSI), Brugg, Switzerland
[6]Federal Agency for Nuclear Control (FANC-AFCN), Bruxelles, Belgium
[7]The Federal Office for the Safety of Nuclear Waste Management (BASE), Berlin, Germany

Correspondence to: Robert Cuss (rjcu@bgs.ac.uk)

Abstract

This paper presents the findings of the Gas Transport (GT) field experiment investigating how Opalinus Clay (OPA) responds to gas pressure at the Mont Terri underground research laboratory in Switzerland. The experiment aimed to determine whether advective gas movement in OPA occurs through visco-capillary flow or through the creation of dilatant gas-filled pathways formed by localised deformation of the clay matrix. A combined strategy was adopted: laboratory studies under controlled conditions were used to inform the design and interpretation of a large-scale field experiment. This paper focuses on the field component, summarising results from the first gas (helium) injection test from Day 447 to 1050. The experiment used a nine-borehole array drilled perpendicular to bedding in Gallery 08. A central borehole served as the gas injection point, while eight surrounding boreholes were instrumented to monitor porewater pressure and rock deformation using fibre-optic sensors, extensometers, and inclinometers. Key outcomes include: 1) Gas entry occurred at 4190 kPa, close to the minimum principal stress. This was followed by a reduction in gas pressure of 960 kPa over 37 days as steady state flow was established. Deformation was mainly down-dip of the injection borehole (towards ~225°), with deformation measured predominantly as borehole-axial strain (perpendicular to bedding), suggesting that the anisotropy of the OPA controlled the propagation of gas along bedding. Overall, the observations are consistent with advective gas movement through the formation of localised dilatant pathways; 2) Increased injection rates triggered a second, more energetic event at 3720 kPa, causing rapid pressure loss and deformation perpendicular to bedding. A large amount of helium was detected at the wellhead of at least four of the monitoring boreholes, confirming gas had reached the observation boreholes and migrated upwards to the gallery. The second event is interpreted as bedding-plane splitting and the creation of a partially open macro-feature with limited flow capacity; 3) A clear transition from dilatant pathway growth to bedding-plane failure demonstrates that gas transport behaviour in OPA depends strongly on injection rate under the GT field-test conditions.

https://doi.org/10.5194/sand-2026-3
Preprint. Discussion started: 25 March 2026

SaND Safety of Nuclear Waste Disposal Discussions

1 Introduction

In a geological disposal facility (GDF) for radioactive waste, hydrogen, carbon dioxide, nitrogen, and hydrogen sulphide will be produced through a range of processes including the corrosion of ferrous materials under anoxic conditions, radioactive decay of the waste, radiolysis of organic materials and water, and the microbial degradation of organic materials (Rodwell et al., 2003). Repositories for radioactive waste are designed and engineered to limit high hydrogen concentration and avoid explosive risk. In the Swiss repository concept, hydrogen is the main gas that will be produced from the corrosion of metals. The production of hydrogen is anticipated to span > 100,000 years post emplacement of the waste over which time the gas will move into the host rock through the combined processes of molecular diffusion and bulk advection. Understanding these processes and the long-term fate and impact of the gas is therefore important in the development of a repository for radioactive waste.

In the Swiss repository concept, the Opalinus Clay formation (OPA), has been proposed as a candidate host-rock for the long-term disposal of the nation's radioactive waste. Much attention has focussed on the OPA, which appears to offer favourable properties for the siting of a repository. These include low hydraulic permeability, small molecular diffusion rates, and a significant retention capacity for radionuclides (Delage et al., 2010). However, these properties, in particular the low permeability of the host rock, can severely restrict the movement of gas which can accumulate (Weetjens & Sillen, 2006; Ortiz et al., 2002; Wikramaratna et al., 1993) until pressure becomes sufficiently large enough to cause gas to enter the surrounding host rock (Harrington & Horseman, 1999).

In a clay-based GDF four primary phenomenological models can be defined to describe gas flow as summarised by Marschall et al. (2005; Fig. 1): (i) gas movement by solution and/or diffusion governed by Henry's and Fick's Laws respectively within interstitial fluids along prevailing hydraulic gradients; (ii) gas flow in the original porosity of the fabric governed by a generalised form of Darcy's Law, commonly referred to as visco-capillary (or two-phase) flow; (iii) gas flow along localised dilatant pathways (micro-fissuring), which may or may not interact with the continuum stress field, the permeability of which is dependent on an interplay between local gas pressure and the effective stress state; and (iv) gas flow along macro fractures similar in form to those observed in hydrofracture activities during hydrocarbon reservoir stimulation, where fracture initiation occurs when the gas pressure exceeds the sum of the minor principal stress and tensile strength.

Two primary modes for advective gas transport through natural mudrocks are therefore expected, as shown by the blue box in Fig.1; (i) visco-capillary flow, where capillary forces must be overridden by migrating gas to allow displacement of the wetting phase, and (ii) the formation of discrete gas-filled pathways by localised consolidation of the clay matrix. The potential for one specific mechanism to prevail is dependent on a range of factors, including the saturation state of the clay and the amount and type of clay present (Levasseur et al., 2021). Natural heterogeneity within clay-hosted repositories may also play an important role in the migration of gas and the mitigation of peak gas pressure (Levasseur et al., 2024). For fully saturated pure clay materials, such as those used in engineered barriers, experimental evidence indicates that gas flow by pathway dilation is

https://doi.org/10.5194/sand-2026-3
Preprint. Discussion started: 25 March 2026

SaND
Safety of Nuclear Waste Disposal
Discussions

the mode of transport. In such cases, significant hydromechanical coupling is observed, which cannot be satisfactorily represented by visco-capillary flow processes.

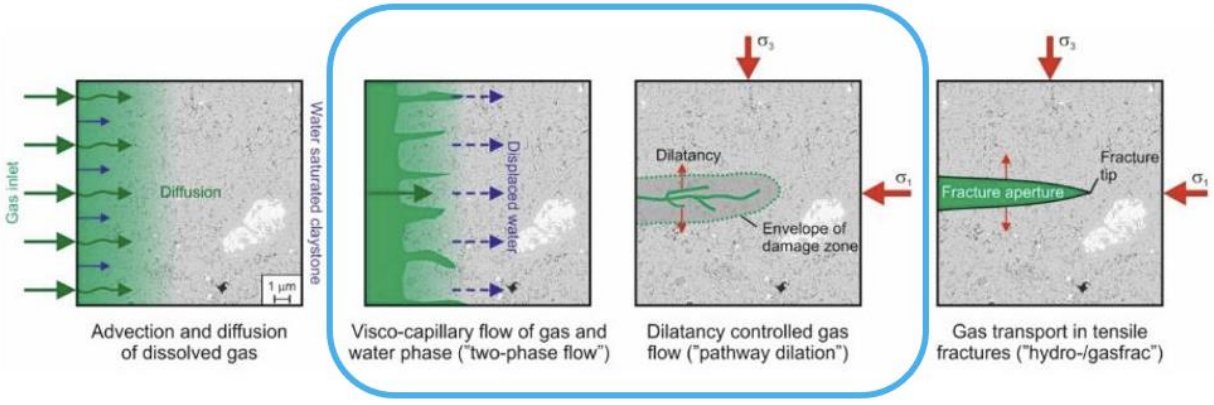

Figure 1: Description of the four main processes of gas movement in clays (after Marschall et al., 2005). The blue box highlights the two mechanisms that the GT experiment aimed to investigate.

Studies suggest that in the case of clay-based rocks gas flows through a series of pressure induced pathways which open and close to allow the passage of gas through the system, the direction of flow is controlled by anisotropy and heterogeneity of the rock (Angeli et al., 2009; Harrington & Horseman, 1999; Horseman et al., 1996, 2004; Harrington et al., 2009, 2013, 2014; Cuss et al., 2014). Understanding these processes and the phenomenological processes which govern the movement of gas has become a priority research area. To understand gas movement in OPA, an experimental study was conducted (Cuss, 2024). Initially, four laboratory experiments were performed to observe gas flow both parallel and perpendicular to bedding. This showed that dilatancy (net volume increase) was seen at the time of gas entry. This was followed by the Gas Transport (GT) in-situ experiment at the Mont Terri Underground Research Laboratory (URL), Switzerland. The GT experiment focused on the characterisation of the physical phenomena describing the gas transport and its mechanical interaction with the surrounding barriers and in particular the further understanding of the creation of micro- and macro-fractures. The experimental programme was designed so that early observations from the laboratory experiments could feed directly into the design and operation of the field test.

Wiseall et al. (2020) reviewed relevant field-scale gas tests conducted in the OPA, as well as the Callovo-Oxfordian claystone in France, to summarise the key findings and lessons learned. This review was used in the design of the current GT test. Several gas injection tests have been conducted at the Mont Terri URL, including the Gas permeability experiment (GP; Marschall et al., 2003), Gas threshold pressure test (Croisé et al., 2006; Marschall et al., 2005), Long term gas injection experiment (GP/GS; Marschall et al., 2003), Gasfrac self-sealing experiment (GS; Marschall et al., 2003), Multi-step gas injection test (GS-2; Marschall et al., 2005), Hydro-gas experiment (HG-A; Lanyon et al., 2009), and HG-B (Xu et al., 2013; Shao & Schuster, 2009). In addition, the Gas threshold pressure test O5 was conducted in the Benken deep borehole in the Northern part of Switzerland. These tests have predominantly concentrated on characterising the hydro-mechanical properties of the OPA using a variety of test set-ups and methodologies. Several tests noted clear evidence of anisotropy in the hydro-mechanical data,

https://doi.org/10.5194/sand-2026-3
Preprint. Discussion started: 25 March 2026

SaND Safety of Nuclear Waste Disposal Discussions

mainly because of the clearly pronounced bedding of the OPA. Evidence of fracturing was observed using techniques such as micro-seismics, ultra-sonic imaging, and resin injection. In terms of the scale of these in situ experiments, the fractures were relatively large features.

2 Experimental setup

The experiment was conducted at the Mont Terri URL, north of the town of St. Ursanne in the canton of Jura (Switzerland) in the shaly facies of the OPA. The laboratory is located 280 m underground and is accessed via a security tunnel, which runs alongside a main highway tunnel through the Jura Mountain range. Taking experience from previous field experiments on borehole spacing and sensor type/distribution, a nine-borehole array was designed, as shown in Fig.2. The nine boreholes were drilled in the floor of Gallery 08 at an orientation of 326/57 so that they were oriented perpendicular to bedding. The length of all boreholes was ~15.5 m with a diameter of 101 mm.

Borehole spacing must be carefully selected. The disturbed zone around boreholes was assumed to be half the borehole diameter, meaning each borehole has a zone of influence of ~200 mm. Boreholes can generally be drilled with a 1% location error, meaning if two boreholes are non-ideally located with a one metre separation between borehole centres, the distance between them would be 500 mm between the central injection borehole and a monitoring borehole, or 260 mm between two monitoring boreholes, as illustrated in Figure 2a. This means that no borehole can "interfere" with any other borehole. Therefore, a separation of one metre was selected between the central injection borehole and the eight monitoring boreholes.

Figure 2 shows the main components of the experimental setup (see Cuss *et al.*, 2024 for full details):

- Injection borehole [green: Borehole BGT-10] equipped with 3-fold packer system; injection interval and intervals below and above monitoring porewater pressure; with fibre-optic (FO) cable clamped at the packers.
- FO [purple: Boreholes BGT-3, 5, 7, 9]: 4 observation boreholes equipped with FO cable only (FutureNeuro™ FN-SILL-3).
- Ext [orange: Boreholes BGT-4, 8]: 2 observation boreholes equipped with chain extensometers (potentiometer) and FO cable.
- Ext/Inc [blue: Borehole BGT-6]: 1 observation borehole equipped with extensometer/inclinometer chain and single-mode FO cable.
- PP [green: Borehole BGT-2]: 1 observation borehole equipped with a 6-fold multipacker system for pore pressure measurements and FO cable clamped at the packers.

The clamped FO cables contain one single-mode in a tight buffered metal tube (BRUSens V4), while the other FO cables contains two single-mode tight-buffered fibres in an embossed sheath (FutureNeuro™ FN-SILL-3).

The FO, Ext, Ext/Inc boreholes were grouted using a low permeable bentonite/cement mixture. All fibre optic cables were interrogated with a high-precision Rayleigh device (Luna ODiSi 6108) to measure axial deformations with a high spatial resolution of ~2 cm and high accuracy/repeatability of 1 microstrain. Figure 2b shows the relative depth of each borehole type. As shown, the sensor array was optimised around the depth of the 500 mm injection interval. At the midpoint of the injection interval there was a corresponding pore pressure, extensometer, and extensometer/inclinometer sensor. The sensor array also

https://doi.org/10.5194/sand-2026-3
Preprint. Discussion started: 25 March 2026

recorded data two metres above and below the injection interval. Note: the fibre optic data coverage was much longer than the other sensors, running along the complete length of the borehole.

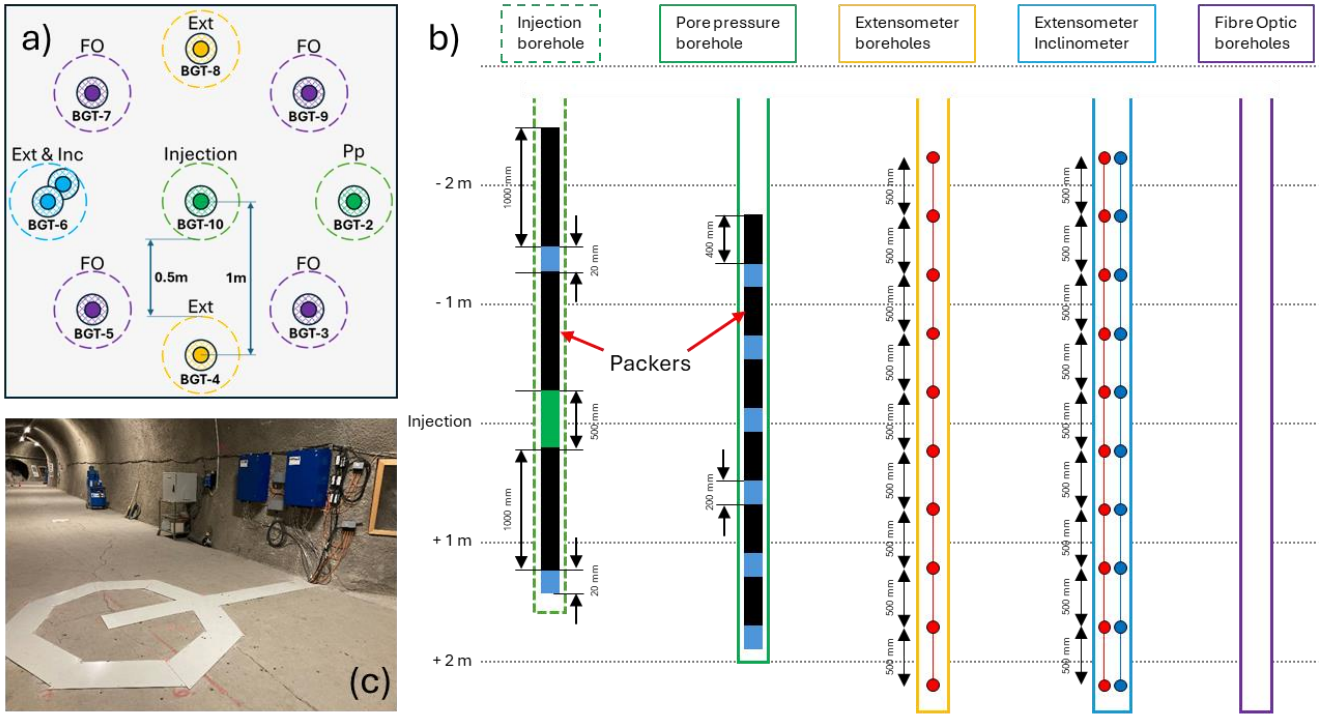

Figure 2 – Experimental setup of the GT experiment. a) Arrangement of the borehole array. The solid colour shows the boreholes, the hatched area shows the borehole disturbed zone (BDZ), the dashed line shows the maximum extent of the BDZ based on drilling uncertainty of 1% of a 15m borehole, as illustrated by BGT-6; b) Instrumentation distribution in the boreholes; c) Photograph of the experimental setup at the Mont Terri URL.

Surface equipment included a digital logger using Solexperts GeoMonitor II (GMII) software, allowing real-time monitoring of data and remote operation of the experimental system. Injection was performed using a large-volume 5 litre water/gas interface vessel connected to a high-precision Teledyne-ISCO 500 series D syringe pump.

The borehole network was drilled sequentially. The pore pressure borehole (BGT-2) was drilled first and sealed off into 6 intervals using packers. The intervals were saturated with artificial porewater (APW) to the expected ambient pressure of ~1000 kPa. This borehole was tested at a depth of 12 m (proposed injection depth, Table 1) and was shown to be undisturbed. Step 2 saw the drilling and instrumentation of the remaining observation boreholes over 4-6 weeks. For each new borehole, the pore pressure in BGT-2 was assessed, with stable pore pressure indicating that the test site was representative of undisturbed OPA. Step 3 was the drilling and instrumentation of the central injection borehole (BGT-10). It took around 2 months to achieve stable pore pressure in BGT-10. No major changes were seen as each successive borehole was drilled and instrumented, giving confidence that the location was sound and appropriate for gas testing.

https://doi.org/10.5194/sand-2026-3
Preprint. Discussion started: 25 March 2026

SaND Safety of Nuclear Waste Disposal Discussions

3 Results

Table 1 lists all experimental and observational events for the GT experiment. The first 447 days of the experiment comprised of re-equilibration, hydraulic testing, and equilibration as described in detail in Cuss et al., 2024. Figure 3 summarises the data prior to gas testing. Figure 3a shows the pressure data for the three intervals in the injection borehole (BGT-10), showing the various experimental stages. Figure 3b shows the initial pressurisation and re-equilibration of BGT-10, showing that pore pressure had reached steady values and that no damage was noted to the borehole. Figure 3c shows the various tests that were conducted to assess the viability of the intervals in BGT-10 and the seven-step hydraulic test conducted from Day 345. The results prior to gas injection are given in detail in Cuss et al. (2024).

Event	Day	Description	Event	Day	Description
0	0	Start of the test		645.87	Start of gas ramp 5
	30.85	Pressure in injection borehole packers increased		654.15	End of gas ramp 5
	43.90	Pore pressure increased in injection intervals		681.29	Start of gas ramp 6
I	204.75	Interval testing – Start of pulse-decay in injection borehole intervals		699.15	End of gas ramp 6
	226.81	Interval testing – Increase in pore pressure in INTP02		713.75	Start of gas ramp 7
	233.54	Interval testing – Start of pressure decay in INTP02		732.98	End of gas ramp 7
	272.68	Interval testing – Increase in pore pressure in INTP01		745.62	Packer pressure increase
	281.81	Interval testing – Start of pressure decay in INTP01		748.90	Start of gas ramp 8
H	345.80	Hydraulic test – Up1	**1.0a**	**751.63**	**Change in pressure gradient**
	346.80	Hydraulic test – Up2	**1.0b**	**751.78**	**Change in pressure gradient**
	349.89	Hydraulic test – Up3	**1.1**	**752.49**	**Change in pressure gradient**
	358.81	Hydraulic test – Up4	**1.2**	**752.61**	**Gas pressure peak**
	379.55	Hydraulic test – Down1	**1.3**	**752.69**	**Change in pressure gradient**
	390.07	Hydraulic test – Down2	1.4	752.76	Pump refill
	393.09	Hydraulic test – Down3		790.97	Accidental increase in flow
	398.71	End of hydraulic testing		792.11	Return to old flow rate
G	447.67	Gas in injection interval		803.40	Start of power cut
	526.88	Start of gas ramp 1		805.79	End of power cut
	540.63	End of gas ramp 1		806.92	Increase in flowrate
	554.88	Start of gas ramp 2		819.13	Increase in flowrate
	569.31	End of gas ramp 2		821.76	Increase in flowrate
	581.87	Packer pressure increase		849.63	Increase in flowrate
	582.84	Start of gas ramp 3		855.95	Increase in flowrate
	585.90	Pause of gas ramp	**2.0**	**858.71**	**Change in pressure gradient**
	590.66	Resumption of gas ramp	**2.1**	**858.74**	**Gas pressure peak**
	599.24	End of gas ramp 3	**2.2**	**858.77**	**Reduction in gas pressure**
	615.01	Start of gas ramp 4	**2.3**	**858.81**	**Large reduction in gas pressure**
	624.58	End of gas ramp 4	S	875.65	End of gas injection (Shut-in)
	640.86	Packer pressure increase			

Table 1: Events during the GT filed test, including Gas Injection Test 1.

3.1 Gas injection test 1

The gas injection test began on Day 447.66 (11th July 2022) and was concluded on Day 875.09 (11th September 2023), a total of 427.43 days. Figure 4a shows the pressure response of BGT-10. The plan was to raise gas pressure in the injection interval

https://doi.org/10.5194/sand-2026-3
Preprint. Discussion started: 25 March 2026

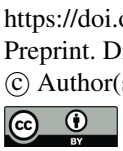

SaND
Safety of Nuclear Waste Disposal
Discussions

by 500 kPa steps over a two-week period using constant injection into the interface vessel under constant flow, hold pressure constant for two-weeks to observe gas flow, and repeat until gas entry occurred, following which gas injection would be continued under constant flow conditions. Seven gas ramps are shown with eight constant pressure periods.

Gas flow rate during the constant pressure hold stages was analysed. Flow converted to standard pressure and temperature (STP) increased from 1.838 $\times 10^{-10}$ m^2/s at 602 kPa to 3.036 $\times 10^{-9}$ m^2/s at 4099 kPa, as shown by the power-law in Fig.4b. Interaction is observed between the injection interval INTP02 of BGT-10 and the pore pressure interval above (INTP03). This has been interpreted as either gas moving upwards or the displacement of pore fluid to INTP03 and not leakage as little change in slope is seen when the pressure in the packers was increased (green dashed lines in Fig.4a). Moreover, coupling observed during hydraulic testing was not as strong, even accounting for the difference in pressure gradient (Fig.3c). There was little correlation with the gas injection pressure in the remaining observation boreholes (Cuss et al., 2024).

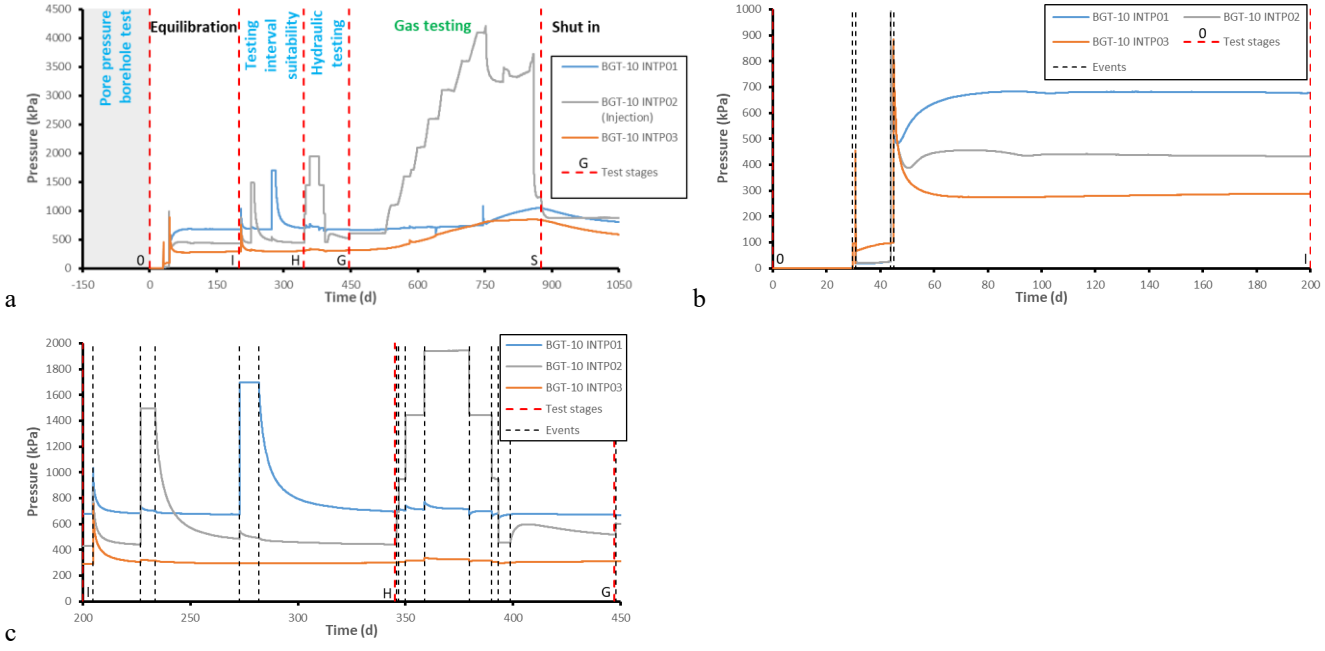

Figure 3: Rehydration, hydraulic and gas testing of BGT-10. a) Summary of the complete test history showing the pore/gas injection pressure response in the three intervals of the injection borehole; b) zoom-in: pore pressure during re-equilibration; c) zoom-in: testing interval suitability and hydraulic testing of the injection interval. See Table 1 for description of test stages.

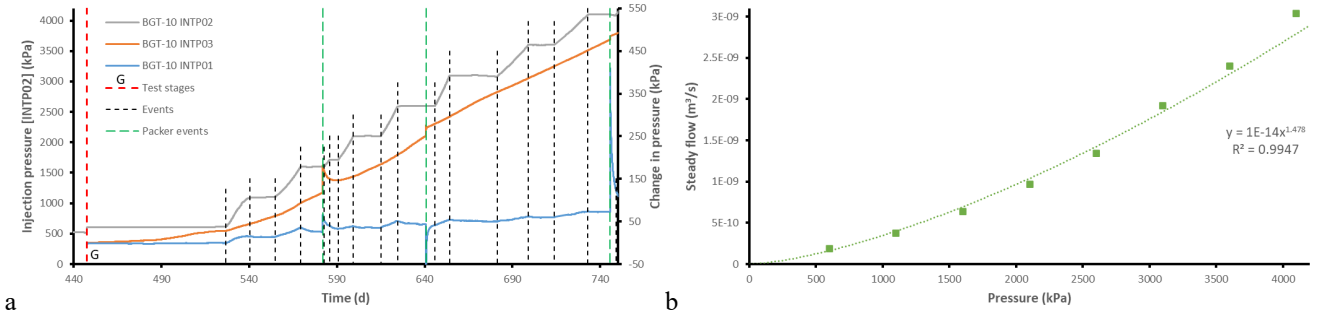

https://doi.org/10.5194/sand-2026-3
Preprint. Discussion started: 25 March 2026

SaND Safety of Nuclear Waste Disposal Discussions

Figure 4: Gas injection steps in BGT-10. a) Pressure measured in the three intervals of BGT-10 showing some coupling between intervals. b) Flow rate observed during each constant pressure step.

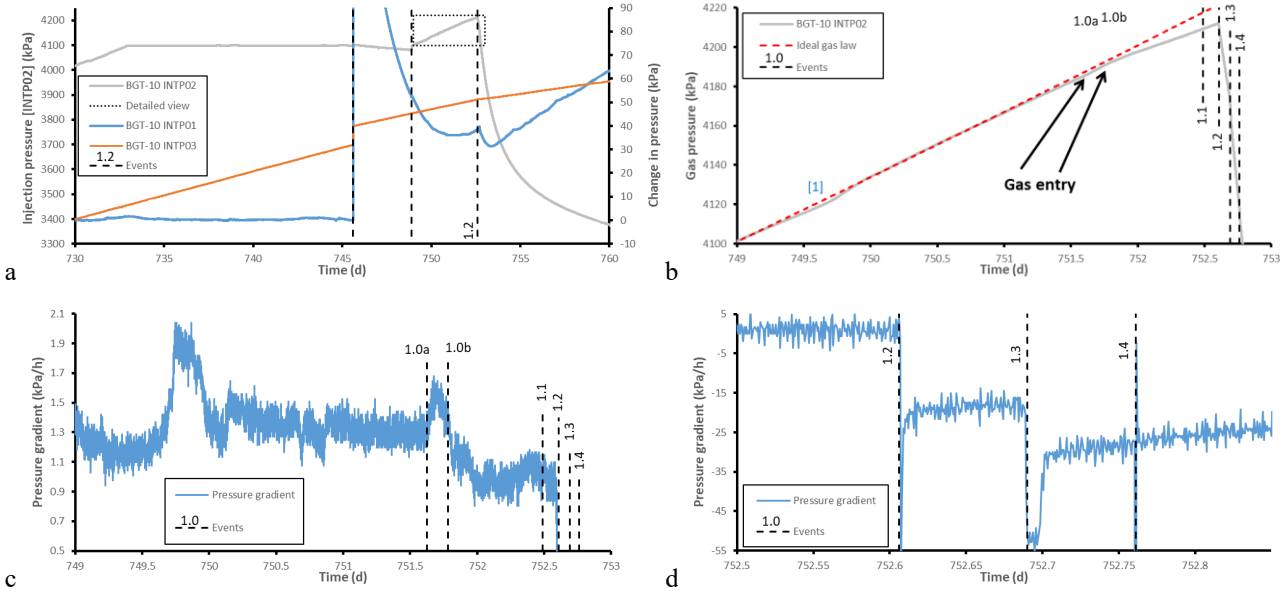

Figure 5: Pore pressure in injection borehole BGT-10 during Event 1. a) Detail of change in pore pressure in BGT-10; b) Detail of gas pressure around the time of gas entry; c) Gas injection pressure gradient; d) Gas injection pressure gradient detail.

3.2 Event 1

The first significant event occurred at Day 752.61 (Fig.5a), when gas pressure peaked at 4210 kPa on the 8th gas pressurisation ramp, some 3600 kPa above the pore pressure in the injection interval at the start of the gas test. Note: the pressure in the packers was increased during Day 745 prior to the start of the final injection pressure ramp, which created a pressure transient in INTP01 of BGT-10 (Fig.5a). Detailed examination of the pressure response (Fig.5b) shows a deviation of the gas injection pressure from the ideal gas law [highlighted 1][1]. This feature corresponds with temperature variation in Gallery 08 of <1 °C and is not interpreted as being the result of gas movement. Two features [1.0a, 1.0b] are highlighted in Fig.5b related to gas entry as identified from the pressure gradient (Fig.5c). These are interpreted as gas entry and occurred at ~4190 kPa. Gas pressure continued to increase and peaked at 4210 kPa at Day 752.61 [1.2], some 20 kPa above gas entry. This correlates with a short-lived spike in the pressure gradient (-59 kPa/h; Fig.5d) as pressure started to rapidly decrease, before the pressure gradient stabilised at approximately -18 kPa/h.

[1] Because of the steady flow seen at the pressure hold stages (Fig.4b), the volume used in the estimation of the gas pressure from the ideal gas law for each ramp has to be adjusted.

https://doi.org/10.5194/sand-2026-3
Preprint. Discussion started: 25 March 2026

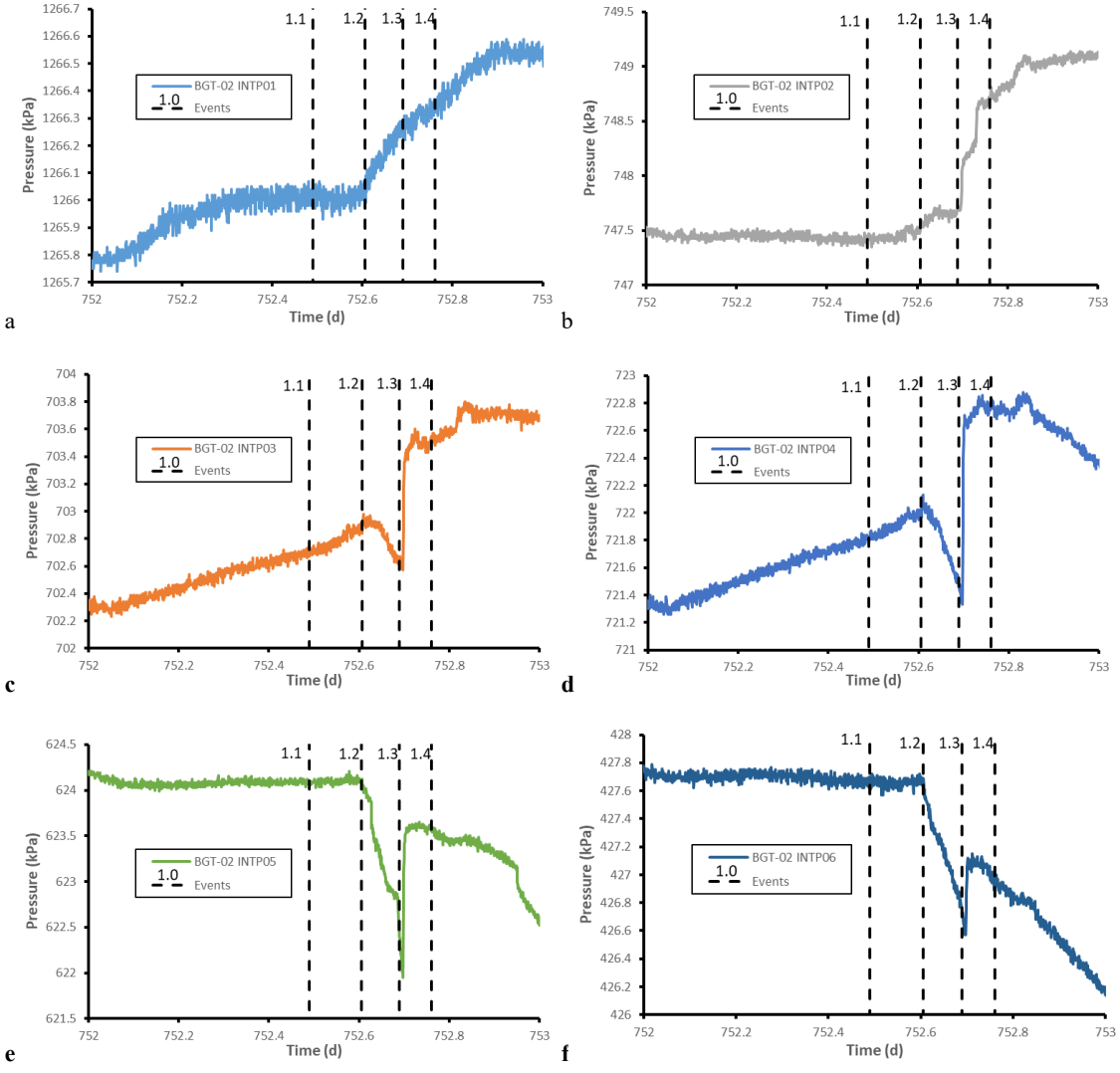

Figure 6: Detail of pore pressure in BGT-2 during Event 1. a) INTP01; b) INTP02; c) INTP03; d) INTP04; e) INTP05; f) INTP06.

A second event [1.3] occurred at Day 752.69, when gas pressure gradient peaked for a second time at -53 kPa/h, before recovering to ~ -30 kPa/h. Figure 5d shows an additional event [1.4] at Day 752.76, although this corresponds with the refilling of the injection pump and is an experimental artefact. The two episodes of increased flow are seen in the injection interval, suggesting that the onset of flow was dynamic. Pore pressure within the injection borehole showed correlation with gas injection pressure [1.2; Fig.5a]. The rate of pressure change varied as a result of both gas movement events in the interval above the injector. Pore pressure marginally increased at peak gas pressure below the injection interval, but showed multiple events around the time of the second gas entry feature [1.3].

Within the pore pressure monitoring borehole (BGT-2; Fig.6), all intervals showed a change at the time of gas peak pressure. The pore pressure started to increase slowly at gas peak pressure in the bottom two intervals of this borehole [Fig.6ab; 1.2].

https://doi.org/10.5194/sand-2026-3
Preprint. Discussion started: 25 March 2026

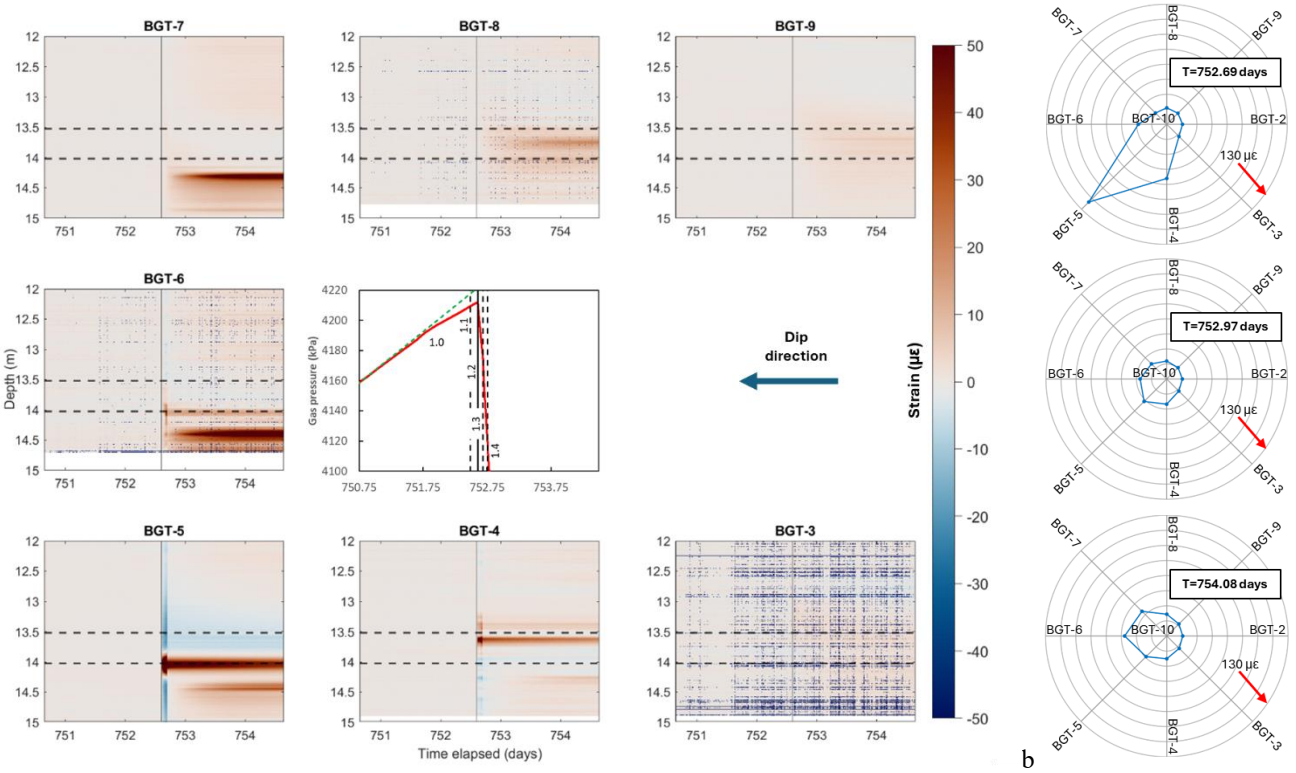

a b

Figure 7: Fibre-optic data for Event 1. a) Waterfall plot showing strain for all boreholes, the position of each plot represents the relative position of the boreholes. Note: horizontal dashed lines show the depth of the injection interval in BGT-10; b) Spider plot showing development of directional strain with time around the injection borehole.

The fibre optic data proved vital in identifying deformation at the time of Event 1 (Fig.7). Deformation predominantly occurred towards BGT-5 and BGT-6 down-dip of the injection borehole. The first identified strain occurred over a 0.3m interval at a depth of ~14m (Fig.7a) in a direction of 225° (Fig.7b), with a spike in strain of ~130 με that lasted less than 20 minutes. Compression is seen over a length of a couple of metres above and below this. During Day 753 a second extension zone developed at a depth of ~14.5m. At this time, strain rotated from an orientation of 225° to 290°. The strain was predominantly extensional, with most boreholes showing compression above and below of a much less magnitude (Fig.7a). As well as a rotation with time, a second extension feature developed in several boreholes some time after gas peak pressure. Close examination of the fibre optic data shows that most boreholes saw a slow build-up of strain, whereas three boreholes showed much quicker development, these three boreholes all showed spikes in strain. The depth of the maximum strain showed that

https://doi.org/10.5194/sand-2026-3
Preprint. Discussion started: 25 March 2026


SaND Safety of Nuclear Waste Disposal Discussions

the zone of influence was oriented at an angle to the borehole array, deepening down dip of the injector. It should be noted that little to no strain was seen up dip (BGT-3, BGT-9).

Only three extensometer sensors showed features that can be reliably correlated with gas movement around the time of gas peak pressure (not shown, see Cuss et al., 2024). In borehole BGT-4, interval EXT02 showed a dilation of ~1 μm, while neighbouring EXT03 showed a decrease of ~8 μm at [1.2]. Further short-lived strain spikes were seen at [1.3] that generally did not result in permanent deformation. In borehole BGT-6 interval EXT02 also showed strain. At [1.1] ~3 μm of compression was seen. The inclinometer data only showed a response at [1.3] in y-offset. This shows that the features seen around gas entry [1.0-1.2] were pure dilatational events, while [1.3] had a component of shear. Generally, the mechanical instrumentation agreed with the observations from the fibre optic boreholes, showing deformation greatest towards 225°.

Gas injection was continued at constant flow following peak gas pressure [1.2]. Figure 8 shows that gas injection pressure reached an asymptote of ~3245 kPa by Day 785, some 32 days following gas peak pressure. The volume of pathways was estimated from the ideal gas law and the measured pressure. This suggests that an equivalent change in volume of at least 1.5l occurred within 2.5 days, with a total of >5l generated by the end of the period[2]. Steady state flow had been established where the flowrate into the wall rock matched the flow into the system.

3.3 Event 2

Figure 8 summarises the main features of Event 2. Figure 8a shows the gas injection pressure and injection pump flowrate between Events 1 and 2. Two experimental incidents occurred around the time that gas pressure reached asymptote. The first at Day 790.97 was human error when gas injection rate was accidentally increased by an order of magnitude, increasing gas pressure by 260 kPa. Flowrate was restored at Day 792.11, creating a slow pressure reduction. The second experimental incident occurred at Day 803.40 when a power cut resulted in injection pausing for 2.39 days. Gas injection was re-established at Day 805.79, resulting in a slowly declining gas pressure. The decision was taken to investigate the role of gas pressurisation rate on the system as gas pressure had reached steady state prior to these experimental events. The injection pump flow rate was increased in steps between 2.46 to 12 ml/h starting on Day 821. This resulted in gas injection pressure increasing from 3320 to 3720 kPa over approximately 40 days.

[2] While estimating pathway volume is a simplification because of pressure variation along pathways, it gives an indication of the minimum volume required to generate pressure reduction.

https://doi.org/10.5194/sand-2026-3
Preprint. Discussion started: 25 March 2026

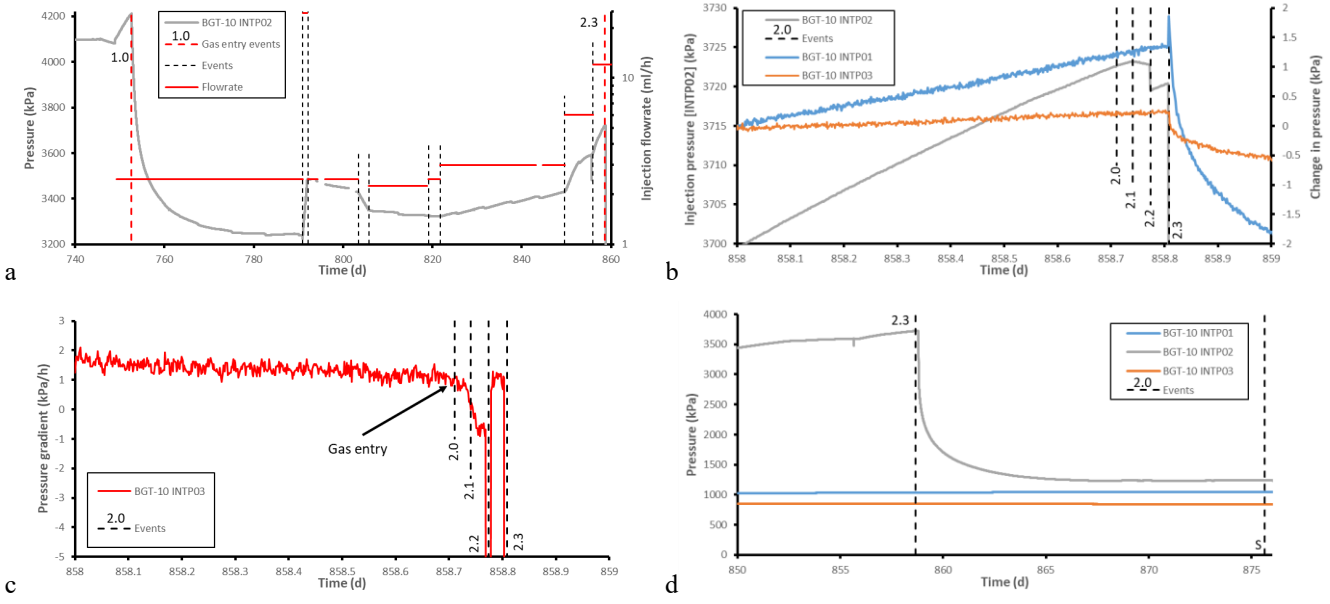

Figure 8: Pore pressure in injection borehole BGT-10 during Event 2. a) Gas injection pressure and flow rate; b) Detail of gas pressure; c) Gas injection pressure gradient; d) Pore pressure up to establishment of steady-state flow.

Increasing gas injection flow rate resulted in an increase of gas pressure and a second gas peak of 3720 kPa on Day 858 (Fig.8b). Close examination of the response of the system showed three distinct events. A change in the pressure gradient (Fig.8c) was seen at Day 858.71 when the gas pressure was 3720 kPa [2.0]. Gas pressure peaked at Day 858.74 at 3720 kPa [2.1]. Gas pressure started to reduce until [2.2] on Day 858.77, gas injection pressure instantaneously reduced by <5 kPa. Gas pressure then started to increase at a similar rate seen before [2.0], when at Day 858.81 with gas pressure of 3720 kPa, gas pressure started to rapidly decrease [2.3].

The four distinct events identified show that Event 2 was a dynamic series of events. At [2.0] gas started to enter the OPA at an elevated rate. This resulted in a peak of gas pressure a short time after, followed by a rapid decrease in pressure. This suggests the formation of an increased volume of gas filled pathway, such as a fracture. Below the injection interval, pore pressure spiked before decreasing. Above the injection interval, Event [2.3] started a reduction in pore pressure. Gas pressure in the injection interval significantly reduced from 3720 kPa at Day 858.81 to 1245 kPa by time of shut in at Day 875.65; this represents a reduction of 2475 kPa in around 10 days. An equivalent volume can be estimated using the ideal gas law, giving an estimated >40l of required volume. Pore-pressure in monitoring borehole BGT-2 showed a variation at [2.3], with changes of <18 kPa seen in all six intervals. Changes in the extensometer data also corresponded with [2.3], with much greater response compared with Event 1.

https://doi.org/10.5194/sand-2026-3
Preprint. Discussion started: 25 March 2026

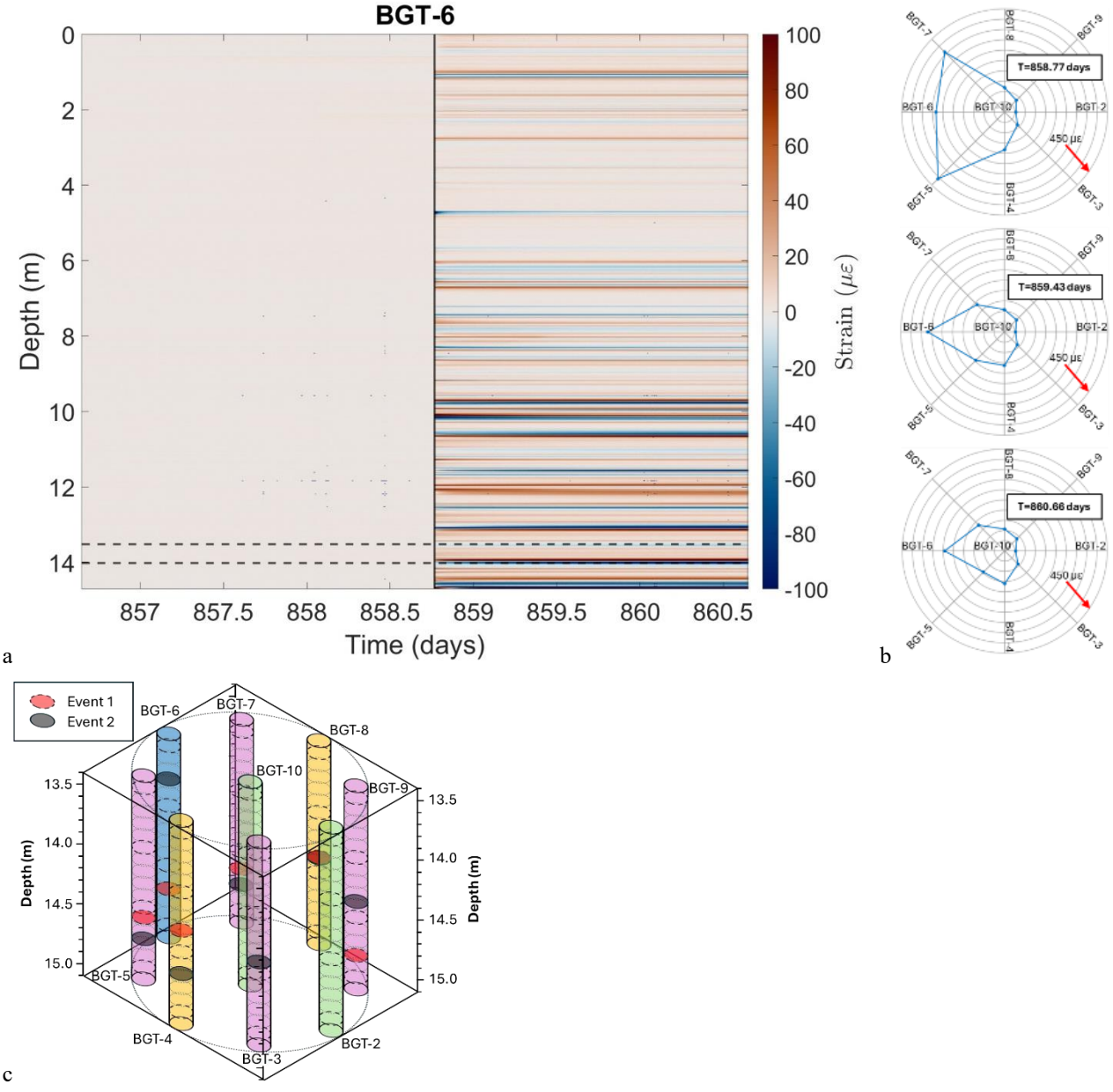

Figure 9: Fibre-optic data for Event 2. a) Waterfall plot of strain in BGT-6; b) Spider plot showing development of directional strain with time around the injection borehole; c) Depth of maximum strain seen during Event 1 and Event 2.

265 Borehole BGT-6 showed extension of up to 94 μm in most sensors (Cuss et al., 2024). The fibre-optic data also showed much more distributed deformation along the borehole lengths in Event 2 compared with Event 1. This was most evident in BGT-6, with deformation seen along the entire length of the borehole (Fig.9a). The build-up of strain was instantaneous and much more rapid than seen in Event 1. Deformation was restricted in extent in Event 1 mainly within a metre of the depth of the

https://doi.org/10.5194/sand-2026-3
Preprint. Discussion started: 25 March 2026

injection interval. This suggests that the mechanism behind Event 2 was fundamentally different from Event 1. Two groups of response are seen in the distribution of borehole responses. In BGT-5 to BGT-7, deformation is seen along the entire length of the borehole, whereas in BGT-3 to BGT-4 and BGT-8 to BGT-9 much more localised deformation was seen, similar to that seen in Event 1. Up to 400 με was seen in the fibre-optic array (BGT-5). The greatest deformation was seen down-dip of the injection borehole, with large positive spikes in strain followed by strain recovery. Along strike of the injection borehole, a less pronounced spike was seen, followed by limited recovery. Limited strain was seen up-dip.

Examining strain as a spider plot (Fig.9b) shows the progression of deformation was very rapid. Strain initially developed down-dip of the injection borehole towards BGT-5 to BGT-7. The strain towards BGT-5 and BGT-7 quickly recovered, meaning that the strain ellipse progressed in the direction of BGT-6, directly down-dip from the injector. Initial deformation was very short-lived down-dip of the injection borehole, with deformation progressing to be predominantly in the direction of BGT-6 (orientation of 270°). Figure 9c shows a representation of the depth of the maximum strain seen in each borehole. The depths of features mostly differed between Event 1 and Event 2, indicating the formation of a new feature.

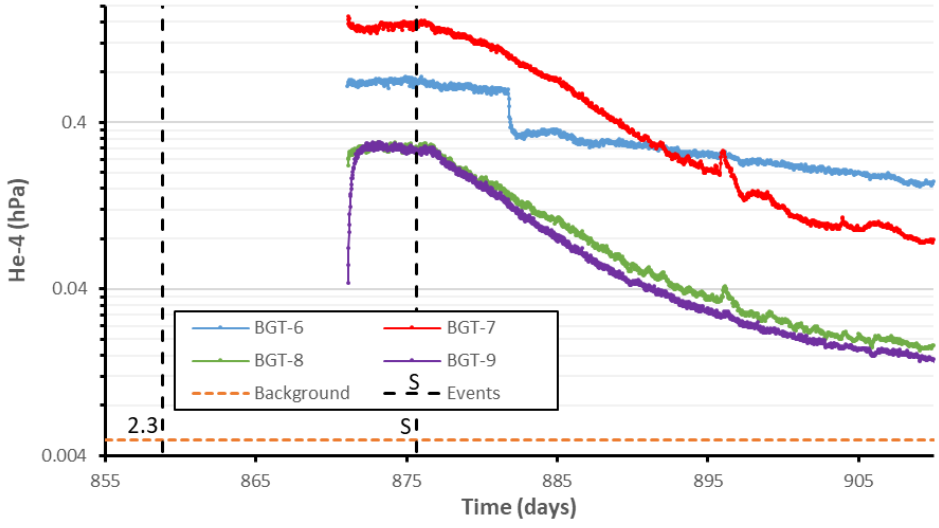

Figure 10: Helium measurements in four monitoring boreholes.

Identification of distributed stain in the fibre optic data along the entire lengths of some boreholes led to a hypothesis that gas had reached the monitoring boreholes and tracked upwards to Gallery 08. A miniRUEDI portable mass spectrometer (Brennwald et al., 2016) was used to measure the helium at the wellhead of four of the monitoring boreholes (BGT-6 to BGT-9), as shown in Fig.10. These all showed elevated levels of helium, between 50 and 350 times the atmospheric background. It must be noted that the experimental setup was not optimised for gas measurement and that quantitative analysis is problematic. However, all four boreholes showed elevated helium at the top of the borehole/gallery floor, demonstrating that gas had directly reached the monitoring boreholes and was venting to the gallery above. The value recorded here is even larger than what was measured as dissolved in formation water (0.002 - 0.2 hPa, Weber et al., 2023). Furthermore, posterior measurements showed that the background value is similar to the atmospheric content and reflecting the gas content of the gallery.

https://doi.org/10.5194/sand-2026-3
Preprint. Discussion started: 25 March 2026

SaND Safety of Nuclear Waste Disposal Discussions

The final stage of the gas injection test was a shut-in. Gas injection was stopped at Day 875.65, and the gas pressure allowed to equilibrate whilst monitoring how the observation boreholes evolved. Gas pressure reduced over a 28-day period to reach a minimum of 870 kPa at Day 903.56; therefore, gas pressure had reduced by 375 kPa because of shut-in.

4 Discussion and interpretation

The aim of the GT experiment was to investigate whether visco-capillary or dilatancy controlled flow predominated in OPA (Fig.1). However, Event 2 showed that Gasfrac was a potential advective gas transport mechanism in OPA.

4.1 What would different flow regimes look like?

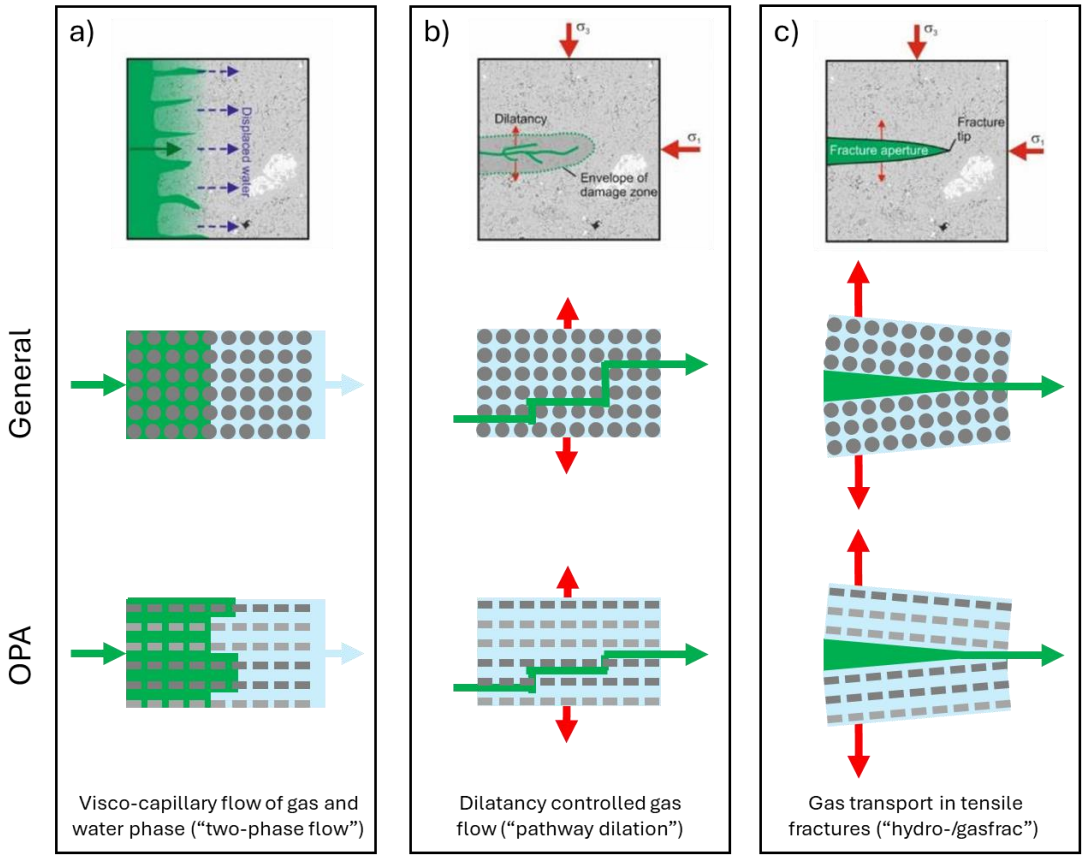

Figure 11: Idealised representation of the three advective gas transport mechanisms expected in Opalinus Clay. a) Visco-capillary flow; b) Dilatancy controlled flow; c) Gas fracture. Note: the sketches do not incorporate the anisotropy and heterogeneity of OPA.

Visco-capillary (VC) flow (Fig.11a): ***General:*** It is easiest to first consider what VC flow would look like in a porous sandstone. If the pore space of the rock is fully saturated, the addition of gas at one end of the rock will displace water once the gas entry pressure has been reached, displacing water from the pore network and out the other end. The gas entry pressure

https://doi.org/10.5194/sand-2026-3
Preprint. Discussion started: 25 March 2026

SaND Safety of Nuclear Waste Disposal Discussions

will be dictated by the size of the pore throats and the viscosity of the fluid in the pore space. In a sandstone, the gas pressure necessary to invoke gas entry is likely to be relatively small and as a result the effective stress acting is not likely to change significantly. Therefore, the overall volume of the rock will not change. In a non-swelling rock, VC flow is generally isovolumetric, with strain only occurring by poroelasticity. ***Opalinus Clay:*** The situation is more complex in a clay-rich rock, such as OPA. The small pore-throats means the gas entry pressure is higher than that expected in a sandstone. Therefore, once gas enters the OPA, the effective pressure is locally perturbed. The displacement of water from the pore space will result in a saturation decrease, which might lead to sample contraction where the pore space in the OPA is now gas filled and the clay dries locally. Gas movement occurs at an elevated pressure. This changes the pore pressure within the OPA, resulting in some swelling that persists while the pore pressure is raised. Therefore, the hydromechanical coupling in OPA will result in some change in volume. This volume change will be felt as far as pore pressure is perturbed. It should be noted that VC flow is not always uniform as the pore network is not homogenous. This can result in viscous fingering resulting in localisation of flow. In Fig.11a the layered nature of OPA results in some layers being more conductive to gas than others.

Dilatancy controlled flow (Fig.11b): ***General:*** Gas flows through the pore network by the pore space expanding, creating localised dilatant pathways. The clay either side of the flow path contracts to accommodate the expanded pathway. However, the clay cannot accommodate all this expansion and macro expansion of the rock occurs. Dilatancy flow is not a fracture mechanics driven process. The bonds between clay grains may be ruptured as the pore network expands. When gas pressure is relieved, the pathways contract by the elastic relaxation around the pathway, suction resulting in fluid movement, and/or creep processes. This can result in the trapping of gas or the full closure of pathways. Microstructural analysis following gas flow by this mechanism often fails to identify flow pathways. The use of nano particles in the gas stream that are larger than the pore throats is one of the few ways to see pathways (Harrington et al., 2012), with clay draped around the particles when gas pressure is relieved. Dilatant gas pathway growth is slow and dictated by the supply rate of gas, interaction with the stress field, and pressure losses along a pathway. Dendritic patterns of flow paths are formed, with multiple pathways forming. If this type of flow was fracture related it would be expected that the growth of the pathway would occur at a rapid rate, with pathways formed at a pressure equal to the local stress plus the tensile strength of the rock. With dilatancy controlled flow, pathways form at a pressure close to the local stress, at a stress much lower than that expected for fracture processes. Dilatancy controlled flow is synonymous with volumetric dilatancy, generally perpendicular to the flow direction, with localised flow channels. ***Opalinus Clay:*** The gas entry pressure of fully saturated OPA is expected to be high. The layered nature of OPA will play a role in the direction of gas transport and therefore the orientation that dilatant behaviour is seen. Pathways will propagate in the direction where dilatancy is easiest and this is likely to follow bedding once gas pathways have become entrapped within weaker layers. Strong anisotropy has been seen in mechanical testing of OPA related to bedding (Winhausen et al., 2023). The induration of OPA is likely to produce strong dilatancy as the clay is not able to compress around the pathway as easily if a normally consolidated clay. It is also likely that gas pathways get "trapped" within layers, as shown in Fig.11b.

Gasfrac (Fig.11c): General: If gas pressure rises sufficiently that it equals the local stress plus the tensile strength of the rock, then fracturing may be invoked. This mechanism is a pure fracture mechanics-controlled phenomenon. Fracture mechanics

https://doi.org/10.5194/sand-2026-3
Preprint. Discussion started: 25 March 2026


SaND Safety of Nuclear Waste Disposal Discussions

states that the fracture will grow at a velocity close to the speed of sound in the rock as long as water can be accessed at the crack tip, which in a saturated rock should be the case. As the crack propagates, strain occurs perpendicular to the direction of growth. If the rock is homogenously stressed, this deformation will be purely tensile and the fracture is a simple opening of the rock. If the stress field is heterogeneous, gas fracturing may result in some shear between the two fracture surfaces. This will result in some strain parallel to the fracture plane. While the fracture is pressurised, it will remain open. As gas pressure is relieved, the fracture will close. The two surfaces of the fracture will no longer perfectly match and therefore closure is not complete, meaning that permanent strain persists. Gas fracturing is therefore synonymous with strain perpendicular with gas movement, with pathway growth being rapid. **Opalinus Clay:** The direction of fracture propagation is controlled by the stress field and the anisotropic nature of OPA. Windhausen et al. (2023) showed marked differences in tensile strength of the OPA with respect to bedding. Therefore, in OPA it is expected that the layering of the rock will strongly influence the direction of fracture propagation. In the scenario of interest for radioactive waste disposal, gas pressure is likely to increase slowly and dilatant pathway flow will be invoked before gas fracture occurs. The latter is only likely to occur if dilatant pathway formation is insufficient to relieve gas pressure over time.

4.2 Interpretation of Event 1

The first gas entry event occurred at a pressure of ~4190 kPa on Day 751, prior to a peak in gas pressure of 4212 kPa. This is consistent with that seen in the laboratory (Cuss et al., 2022; Cuss, 2024), when a deviation from the ideal gas law showed that gas was exiting the injection circuit. In the field test this could be leakage along the borehole/packer interface. However, in GT the pressure within the packer was significantly greater than the gas injection pressure and no evidence of direct gas movement was seen in the pressure response in the intervals above and below the injection interval. As with laboratory tests, this event was not accompanied by any mechanical response and was only noted from the gas injection pressure. Gas peak pressure was seen to be 3600 kPa above the pore pressure in the injection interval prior to gas testing. In laboratory testing the gas entry/peak pressure occurred close to the minimum principal stress. This is well constrained within a laboratory test but is not in GT. Modelling of a nearby experiment had suggested that the three principal stresses at the GT site would be 3.8, 4.7, and 5.3 MPa (Guglielmi et al., 2020). Therefore, gas entry occurred at a pressure greater than the minimum principal stress, but less than the intermediate stress. Bock (2000) report a tensile strength perpendicular and parallel to bedding of 1MPa and 2 MPa respectively. Wild et al. (2015) report tensile strength between ~1 MPa and 3 MPa, while Winhausen et al. (2023) report tensile strength between 1.1 and 2.4 MPa dependent on the orientation of the fracture with respect to bedding. Fracture mechanics dictates that the OPA would fail in a tensile manner when the pressure was equal to the minimum principal stress plus tensile strength; therefore, when excess pressure equals the tensile strength. If the minimum principal stress is 3.8 MPa and the peak gas pressure is 4.21 MPa, the excess pressure is ~0.41 MPa, considerably lower than previously reported tensile strengths. As the minimum principal stress is poorly constrained, it is uncertain whether the gas injection pressure reached a level expectant to result in tensile fracturing of the rock. However, the gas pressure was close to the modelled stress field and

https://doi.org/10.5194/sand-2026-3
Preprint. Discussion started: 25 March 2026


SaND Safety of Nuclear Waste Disposal Discussions

therefore gas peak pressure has been interpreted as being similar in the field and laboratory and not the result of a fracturing process.

The mechanical extensometer data showed small strains parallel to the borehole axis, i.e. perpendicular to bedding at gas peak pressure. The fibre-optic data confirms this, with initial strain occurring towards BGT-5 and BGT-6 downdip of the central injection borehole. The initial spike in deformation recovered and the deformation rotated towards BGT-6, directly down dip of the injection borehole. The development of strain was relatively slow and took over 24-hours to develop fully. This is not indicative of a fracturing process and is like what would be expected for the formation and development of strain associated with dilatant pathway formation. The response has a hydrodynamic origin, although no porewater pressure variation was seen in BGT-2.

Gas pressure reduced to an asymptote of ~3245 kPa following gas peak pressure. This is greatly more than the pore pressure at the injection interval and is common with the observations of laboratory testing. Steady state flow can be confirmed within the laboratory where inflow and outflow are known to match. This is not possible in a field test where the far-field flow is an unknown. However, as the behaviour is common between the laboratory and the field-scale, it is therefore interpreted that dilatant pathways were formed at the time of gas peak pressure and that these pathways continued to develop until a stable growth rate was achieved.

Changing the injection flow rate caused the gas pressure to rise, and when the flow rate was reduced the pressure stabilised at a different long-term level (a different asymptote). This is consistent with the conceptual model of the development of dilatant pathways. Once gas was mobile within the rock mass, no further significant deformations were noted. If tensile fracture had occurred it would be expected that further strain would be observed, especially as gas flowed towards the observation boreholes. The fibre-optic and extensometer sensors only recorded the entry of gas at the peak pressure.

If gas movement was through pure two-phase flow, it wouldn't be expected that strain at gas entry would be observed instantaneously. The flushing of porewater away from the injection interval would also result in the raising of porewater pressure at the monitoring borehole and further deformation as the movement of water would result in a raising of porewater pressure and increased swelling. Two-phase flow also results in the desaturation of the rock as water is flushed from the pore space. Testing within the laboratory noted no measurable desaturation and that is expected in the field test as all observations are consistent between the laboratory and field scales.

Considering all observations of the field test and comparing with the more constrained laboratory test, Event 1 has been interpreted as the formation of dilatant pathways and the development of stable pathway growth at a rate related to the gas injection rate. The pressure at which the dilatant pathways formed was controlled by the local stress field, while the direction of propagation was controlled by the anisotropic nature of the OPA. Pathways have formed following bedding in a downdip direction showing that gas movement is controlled by a combination of stress and material anisotropy.

https://doi.org/10.5194/sand-2026-3
Preprint. Discussion started: 25 March 2026


SaND Safety of Nuclear Waste Disposal Discussions

4.3 Interpretation of Event 2

The signature of Event 2 was different from that seen in Event 1, most notably the time that changes occurred. Increasing the flow rate into the injection interval resulted in an increase in gas pressure and a secondary peak at 3723 kPa, this was 489 kPa lower than the first gas peak pressure, close to the modelled value of minimum principal stress of 3800 kPa. The lowering of the gas peak pressure could suggest a re-activation of a feature created in Event 1. As an example, creation of a fracture in shear occurs at a higher stress than the reactivation of sliding. In this example the first event of breaking virgin rocks takes more energy than it does to slide along an already broken rock. However, repeat gas testing does not always see this behaviour. In the Lasgit field test in Sweden (Cuss et al., 2026), repeat gas injection testing into a compacted bentonite system occurred at successively higher gas pressures. This may be attributed to continued developing stresses within the bentonite, but once stress levelled, this increasing gas pressure was still seen. Gas movement at Lasgit was attributed to the formation of dilatant gas pathways as gas was observed to move to individual sensors and could have only done so through localised flow pathways. No weakening of the bentonite was seen by successive gas flow events. Repeat gas injection of OPA was partially investigated in the laboratory as part of the GT test programme (Cuss et al. 2022). The first gas injection event occurred at a stress state close to the confining pressure. Increasing confining pressure resulted in a secondary peak gas pressure also close to confining pressure. In both stages of the experiment, gas peak pressure occurred close to the minimum principal stress and no weakening of the OPA was seen. Therefore, taking all these experimental observations into account, the reduction in gas peak pressure was not expected and not indicative of weakening of the OPA by dilatant pathway formation and propagation.

Comparing the fibre optic data for Event 1 and Event 2 shows broadly similar responses, with notable differences. In Event 2, the deformation occurred in a similar direction to Event 1, but the depth of the observed strain was different and was much quicker to develop. In the first event, the development in strain as noted by the fibre optic data in BGT-7 was slow to develop, taking around 36 hours for the strain to plateau (Fig.12). This is in comparison to around 5 minutes seen in Event 2. Deformation was seen all along the borehole in some boreholes as opposed to localised deformation seen in Event 1. Therefore, the physics driving these two events differs, as does the energy released by them; Event 2 is a much more energetic and rapid event. Therefore, it is discounted that the second event is created by a rapid increase in dilatant pathways.

The results from the miniRUEDI showed that gas had reached at least 4 of the monitoring boreholes. This explains why deformation is seen in the fibre-optic data for a much broader range of depths. Gas reached the boreholes and rapidly migrated upwards through the grout material and into the gallery above. This showed that gas moved to multiple observation boreholes. If this was through localised dilatant pathways, it is unlikely that gas would reach the four boreholes at the same time and result in such rapid deformation in multiple locations, as shown by the strain seen in fibre-optic data. Therefore, Event 2 is better described as a gas fracture, possibly forming as a bedding plane split. A fracture/bedding plane split would explain the rapid deformation and the migration of gas to multiple observation boreholes at the same time. The final observation in favour of a fracturing-type process is the reduction in gas pressure of 2475 kPa over a 10-day period to 1240 kPa, compared with a reduction of 960 kPa to 3250 kPa over 37 days for Event 1. Event 2 shows a significant reduction in gas pressure to a pressure

https://doi.org/10.5194/sand-2026-3
Preprint. Discussion started: 25 March 2026

SaND Safety of Nuclear Waste Disposal Discussions

close to pore pressure. This shows a lack of capillary pressure and suggests a fracture. During shut-in more pressure was lost, which suggests that the flow of gas through the open fracture was limited to an extent. However, the lack of capillary pressure suggests the formation of a macro scale feature and not a micro-scale porosity-based one. Therefore, Event 2 is concluded to be a macro-fracture. However, a gas fracture would require a gas pressure equal to the local stress field plus tensile strength, and failure occurred at a much lower pressure. Therefore, the formation of this feature was not a pure gas fracture process and must have occurred at sub-critical stress and is therefore interpreted as a bedding-plane split. This shows that the anisotropic nature of OPA has influenced fracture formation with the weakest plane being located parallel with bedding. Why the bedding plane split occurred at a sub-critical pressure is unclear and will be investigated in follow-up laboratory experiments.

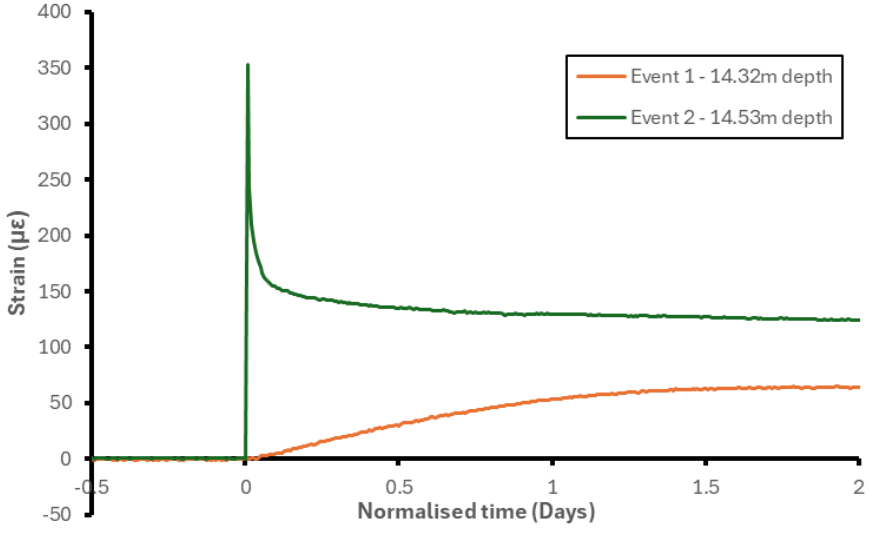

Figure 12: Fibre-optic strain data from borehole BGT-7 at the time of Event 1 and 2 showing the difference in magnitude of strain and rate of strain development.

One consideration is whether the migration of gas to one observation borehole and the rapid flow of gas into the borehole resulted in the formation of the bedding plane split. The time resolution of the data is insufficient to fully describe whether a series of events resulted in the rapid formation of the split and this remains a possibility. Even without fully describing the series of events that resulted in Event 2, a transition from dilatancy controlled flow to a fracture-dominated splitting process was seen with increased gas injection rate. This suggests that the transition from dilatancy controlled flow to gas fracture is controlled by the rate of gas injection.

5 Conclusions

The GT experiment aimed to provide evidence on the mechanism(s) governing advective gas flow in Opalinus Clay under the boundary conditions of the Mont Terri field test, and in particular whether advective flow was dominated by visco-capillary flow through the intact clay matrix or by the formation of localized gas-filled pathways associated with dilatant deformation. A field test comprising 8 monitoring boreholes around a central injection borehole was seen to perform well.

https://doi.org/10.5194/sand-2026-3
Preprint. Discussion started: 25 March 2026


SaND Safety of Nuclear Waste Disposal Discussions

The gas injection test was conducted as a series of pressure ramps of 500 kPa over a two-week period, with pressure held constant for a further two-weeks to monitor flow at constant pressure. Gas entry occurred at a pressure of ~4190 kPa on Day 751, prior to a peak in gas pressure of 4212 kPa at Day 752.61. This was followed by a reduction in gas pressure, which reached asymptote of ~3245 kPa after 37 days: a reduction of ~960 kPa. This behaviour was consistent with that observed in the laboratory, where gas entry occurred at close to the minimum principal stress in four experiments. Two dynamic flow events were observed: the first featured a brief spike in gas flow followed by stabilisation, while the second showed a peak in the gas pressure gradient. Pore pressure changes correlated with these gas movement events, indicating a complex coupled hydro-mechanical interaction.

Fibre optic measurements were crucial in identifying deformation patterns, primarily showing extensional strain down-dip from the injection borehole. Deformation was most significant towards 225°, in the direction of dip. The perturbations from gas pressure changes were mostly short-lived, lasting less than five days. This first event is interpreted as the formation of dilatant gas pathways, with stable pathway growth.

Gas injection rate was increased in steps, resulting in a second peak in gas pressure at 3723 kPa, some 489 kPa lower than the first peak in gas pressure and close to the modelled minimum principal stress of 3800 kPa. This event was much more energetic, resulting in a reduction in gas pressure of 2475 kPa over a 10-day period to 1240 kPa, close to the pore water pressure. The response from all sensors was much quicker, with strain developing in the order of 10-minutes compared with 36 hours for the first gas peak. Deformation was observed perpendicular to bedding, predominantly down-dip of the injection borehole in a direction of 270°. It was evident that gas had reached the monitoring boreholes, and this was confirmed using a portable mass spectrometer (miniRUEDI), which showed elevated levels of helium between 50- and 350-times background in four of the monitoring boreholes. This second gas event has been interpreted as a bedding plane split at sub-critical stress and the formation of a macro-scale partially open feature, consistent with the large reduction in gas pressure and the implied loss of capillary control. The feature had limited flow capability as shut-in resulted in a further reduction in gas pressure as the helium drained to the observation boreholes. A transition was observed from stable dilatant pathway growth to bedding plane splitting with increasing gas injection rates. This suggests that the physics of advective gas movement is injection rate dependent under the conditions of the GT field test.

Within the conditions of the GT in-situ test at Mont Terri, the observations are not consistent with advective gas transport being dominated by visco-capillary flow through the intact clay matrix. Instead, gas migration is accommodated mainly by localized pathway development, transitioning from stable dilatant pathways to bedding-plane splitting at higher injection rates. It is emphasised that the GT experiment represents a site-specific field test conducted under defined boundary conditions at the Mont Terri URL. Observed gas transport pathways and deformation responses may be influenced by experimental factors, including borehole geometry, grouting, and gallery boundary conditions. Consequently, the results should be interpreted as process-level insights rather than direct indicators of repository integrity, and their relevance to disposal concepts requires evaluation within integrated safety assessment frameworks.

https://doi.org/10.5194/sand-2026-3
Preprint. Discussion started: 25 March 2026

SaND Safety of Nuclear Waste Disposal Discussions

Acknowledgements

The authors would like to thank the many people who have contributed to the GT field experiment, including Andy Wiseall (now at Nuclear Waste Services), Christophe Nussbamn and all the staff at Mont Terri that have assisted in the project, Thomas Fierz, Benjamin Helmlinger, and Ursula Rösli of SolExperts, Dorothee Rebscher, Hua Shao, and Vinay Kumar of BGR, Elke Jacops of SCK-CEN for diffusion experiments, and Andres Idiart of Amphos21 for modelling work during the experimental design phase. This paper is published with the permission of the Executive Director, British Geological Survey (NERC).

References

Angeli, M., Soldal, M., Skurtveit, E., and Aker, E. (2009). Experimental percolation of supercritical CO2 through a caprock. Energy Procedia, 1, 3351–3358.

Bock, H. (2000). RA experiment: data report on rock mechanics—Mont Terri project. Technical report Nagra, Internal report TN00-02, Q+S Consult, Germany; 2000

Brennwald, M. S., Schmidt, M., Oser, J., and Kipfer, R.: A portable and autonomous mass spectrometric system for on-site environmental gas analysis, Environ. Sci. Technol., 50, 13455–13463, https://doi.org/10.1021/acs.est.6b03669, 2016.

Croisé, J., Mayer, G., Marschall, P., Matray, J.M., Tanaka, T. and Vogel, P. (2006). Gas threshold pressure test performed at the Mont Terri Rock Laboratory (Switzerland): experimental data and data analysis. Oil & Gas Science and Technology-Revue de l'IFP, 61(5), pp.631-645.

Cuss, R.J., Harrington, J.F., and Sellin, P. (2026) The evolution of gas migration properties in a field-scale bentonite engineered barrier system; results from six gas tests in the Large Scale Gas Injection Test (Lasgit). Environmental Geotechnics.

Cuss, R.J., Harrington, J.F., and Sentis, M. (2022) Evaluation of gas transport models and of the behaviour of clay rocks under gas pressure: GT Experiment. Mont Terri Consortium Technical Meeting TM-39 JANUARY 2022.

Cuss, R.J., Harrington, J.F., Giot, R., and Auvray, C. (2014). Experimental observations of mechanical dilation at the onset of gas flow in Callovo-Oxfordian claystone. In: Clays in Natural and Engineered Barriers for Radioactive Waste Confinement; Norris, A., Bruni, J., Cathelineau, M., Delage, P., Fairhurst, C., Gaucher, E.C., Hohn, E.H., Kalinichev, A., Lalieux, P, and Sellin, P. (Eds), 400, Geological Society Special Publications: London, United Kingdom, Geological Society of London, pp. 507-519, doi:10.1144/SP400.26

Cuss, RJ (2024). GT laboratory test 3: Description of test results for the DECOVALEX-2027 HyMAR task. British Geological Survey Open Report, OR/25/033. 55pp.

Cuss, RJ, Bird, EJM, Gisiger, J, Rinaldi, A., Harrington, JF, Magri, F, Bernier, F, and Sentis, M (2024). Gas Transport Models and behaviour of Opalinus Clay (OPA) to gas pressure (GT): Field test results. British Geological Survey Commissioned Report, CR/24/117. 124pp.

Delage, P., Cui, Y.J. and Tang, A.M., 2010. Clays in radioactive waste disposal. Journal of Rock Mechanics and Geotechnical Engineering, 2(2), pp.111-123.

Guglielmi, Y., Nussbaum, C., Rutqvist, J., Cappa, F., Jeanne, P. and Birkholzer, J., 2020. Estimating perturbed stress from 3-D borehole displacements induced by fluid injection in fractured or faulted shales. Geophysical Journal International, 221(3), pp.1684-1695.

Harrington, J.F. and Horseman, S.T. (1999). Gas transport properties of clays and mudrocks. In: Muds And Mudstones: Physical And Fluid Flow Properties (eds A.C.Aplin, A.J. Fleet, and J.H.S. Macquaker). Geological Society of London, Special Publication No. 158, 107-124.

Harrington, J.F., Cuss, R.C., Noy, D.J. and Talandier, J. (2014). Processes governing advective gas flow in the Callovo Oxfordian Claystone (COx). Fourth EAGE Shale Workshop, Porto, Spain, 6–9 April, 2014, https://doi.org/10.3997/2214-4609.20140026

Harrington, J.F., Milodowski, A.E., Graham, C.C., Rushton, J.C. and Cuss, R.J. (2012). Evidence for gas-induced pathways in clay using a nanoparticle injection technique. Mineralogical Magazine, 76(8), pp.3327-3336.

Harrington, J.F., Noy, D.J. and Cuss, R.J. (2013). Long-Term Gas Migration Experiments in Callovo-Oxfordian Claystone. British Geological Survey, Technical Report, CR/13-088.

https://doi.org/10.5194/sand-2026-3
Preprint. Discussion started: 25 March 2026

Harrington, J.F., Noy, D.J., Horseman, S.T., Birchall, J.D. and Chadwick, R.A. (2009) Laboratory study of gas and water flow in the Nordland Shale, Sleipner, North Sea. In: Grobe M., Pashin J.C. & Dodge R.L. (eds) Carbon Dioxide Sequestration in Geological Media – State of the Science. AAPG Studies in Geology, 59, 521–543.

Horseman, S.T., Harrington, J.F., and Sellin, P. (1996) Gas migration in Mx80 buffer bentonite. In: Symposium on the Scientific Basis for Nuclear Waste Management XX, Boston, MA, USA. Materials Research Society, 465, 1003–1010.

Horseman, S.T., Harrington, J.F., and Sellin, P. (2004) Water and gas flow in Mx80 bentonite buffer clay. In: Oversby V.M. & Werme L.O. (eds) Symposium on the Scientific Basis for Nuclear Waste Management XXVII (Kalmar), 15–19 June, 2003. Materials Research Society, 807, 715–720.

Lanyon, G.W., Marschall, P., Trick, T., de la Vaissiere, R., Shoa, H. and Leung, H., (2009). Hydromechanical evolution of damage zones around a mictotunnel in a claystone formation of the Swiss Jura Mountains. In: 43rd U.S. Rock Mechanics Symposium & 4th U.S. – Canada Rock Mechanics Symposium, 28 June to 1 July 2009, Asheville, NC, 652–663, paper 09-333.

Levasseur, S., Collin, F., Daniels, K., Dymitrowska, M., Harrington, J., Jacops, E., Kolditz, O., Marschall, P., Norris, S., Sillen, X. and Talandier, J., 2021. Initial state of the art on gas transport in clayey materials. Deliverable D6.1 of the HORIZON 2020 project EURAD, Work Package Gas. EC Grant agreement no: 847593..

Levasseur S., Collin F., Dymitrowska M., Harrington J., Jacops E., Kolditz O., Marschall P., Norris S., Sillen X., Talandier J., Truche L. and Wendling J. (2024). State of the Art on Gas Transport in Clayey Materials – Update 2023. Deliverable D6.2 of the HORIZON 2020 project EURAD, Work Package Gas. EC Grant agreement no: 847593.

Marschall, P., Croisé, J., Schlickenrieder, L., Boisson, J.Y., Vogel, P. and Yamamoto, S. (2003). Synthesis of hydrogeological investigations at the Mont Terri site (Phases 1 - 5). Mont Terri Technical Report TR 2001-02, Geotechn. Inst. Ltd., Bern, Switzerland

Marschall, P., Horseman, S. and Gimmi, T. (2005). Characterisation of gas transport properties of the Opalinus Clay, a potential host rock formation for radioactive waste disposal. Oil & gas science and technology, 60(1), pp.121-139.

Ortiz, L., Volckaert, G. and Mallants, D. (2002). Gas generation and migration in Boom Clay, a potential host rock formation for nuclear waste storage. Engineering Geology, 64, 287-296.

Rodwell, W., Norris, S., Cool, W., Cuñado, M., Johnson, L., Mäntynen, M., Müller, W., Sellin, P., Snellman, M., Talandier, J. and Vieno, T. (2003). A thematic network on gas issues in safety assessment of deep repositories for radioactive waste (GASNET). European Commission EC.

Shao, H. and Schuster, K. (2009) Permeability Measurements of Opalinus Clay (Mont Terri) HG-B: Combined Permeability Tests and Borehole Seismic Measurements. B.1-10856/2009.BGR, Hanover.

Weber, U.W., Rinaldi, A.P., Roques, C., Wenning, Q.C., Bernasconi, S.M., Brennwald, M.S., Jaggi, M., Nussbaum, C., Schefer, S., Mazzotti, M. and Wiemer, S., 2023. In-situ experiment reveals CO2 enriched fluid migration in faulted caprock. Scientific Reports, 13(1), p.17006.

Weetjens, E. and Sillen, X. (2006). Gas Generation and Migration in the Near Field of a Supercontainer-Based Disposal System for Vitrified High-Level Radioactive Waste, Proc. 11th Int. High-Level Radioactive Waste Management Conf. (IHLRWM), Las Vegas, Nevada, April 30–May 4, 2006.

Wikramaratna, R.S., Goodfield, M., Rodwell, W.R., Nash, P.J. and Agg, P.J. (1993) A preliminary assessment of gas migration from the copper/steel canister (No. SKB-TR--93-31). Swedish Nuclear Fuel and Waste Management Co.

Wild, K.M., Wymann, L.P., Zimmer, S., Tjoeny, R. and Amann, F. (2015) Water retention characteristics and state-dependent mechanical and petro-physical properties of a clay shale. Rock Mechanics and Rock Engineering, 48, pp.427-439.

Winhausen, L., Kha;edi, K., Jalali, M., Bretthauer, M., and Amann, F. (2023). The anisotropic behavior of a clay shale: Strength, hydro-mechanical couplings and failure processes. Journal of Geophysical Research: Solid Earth, 128, e2023JB027382. https://doi. org/10.1029/2023JB027382

Wiseall, A.C., Cuss, R.J., and Harrington, J.F. (2020) A review of in situ field tests on the Opalinus Clay and Callovo-Oxfordian Claystone; key findings and lessons learned. British Geological Survey External Report, CR/20/029. 27pp.

Xu, W., Shao, H., Hesser, J., Wang, W., Schuster, K. and Kolditz, O. (2013) Coupled multiphase flow and elasto-plastic modelling of in-situ gas injection experiments in saturated claystone (Mont Terri Rock Laboratory). Engineering Geology, 157, 55-68.